J Neurophysiol 115: 992–1002, 2016.
First published December 16, 2015; doi:10.1152/jn.00699.2015.

Grids from bands, or bands from grids? An examination of the effects of single unit contamination on grid cell firing fields

Z. Navratilova,[1,2] K. B. Godfrey,[1] and B. L. McNaughton[2,3]

[1]*Neuroelectronics Research Flanders, KU Leuven, Leuven, Belgium;* [2]*Department of Neuroscience, Canadian Center for Behavioral Neuroscience, The University of Lethbridge, Lethbridge, Canada; and* [3]*Center for the Neurobiology of Learning and Memory, University of California at Irvine, Irvine, California*

Submitted 15 July 2015; accepted in final form 11 December 2015

Navratilova Z, Godfrey KB, McNaughton BL. Grids from bands, or bands from grids? An examination of the effects of single unit contamination on grid cell firing fields. *J Neurophysiol* 115: 992–1002, 2016. First published December 16, 2015; doi:10.1152/jn.00699.2015.—Neural recording technology is improving rapidly, allowing for the detection of spikes from hundreds of cells simultaneously. The limiting step in multielectrode electrophysiology continues to be single cell isolation. However, this step is crucial to the interpretation of data from putative single neurons. We present here, in simulation, an illustration of possibly erroneous conclusions that may be reached when poorly isolated single cell data are analyzed. Grid cells are neurons recorded in rodents, and bats, that spike in equally spaced locations in a hexagonal pattern. One theory states that grid firing patterns arise from a combination of band firing patterns. However, we show here that summing the grid firing patterns of two poorly resolved neurons can result in spurious band-like patterns. Thus, evidence of neurons spiking in band patterns must undergo extreme scrutiny before it is accepted. Toward this aim, we discuss single cell isolation methods and metrics.

spike sorting; grid cells; medial entorhinal cortex

THE HIPPOCAMPUS CONTAINS "place cells," which fire when an animal is moving around in specific parts of an environment (O'Keefe and Dostrovsky 1971). Several associated regions contain "head-direction cells," which fire when the animal is facing or moving in a specific direction, regardless of location (Ranck 1984; Taube et al. 1990). More recently, "grid cells," which fire in a rhomboidal (aka triangular or hexagonal) lattice (Fyhn et al. 2004; Hafting et al. 2005) over an environment, and "border cells," which fire near environmental boundaries (Savelli et al. 2008; Solstad et al. 2008), have been discovered in the medial entorhinal cortex (MEC), an area that projects directly to the hippocampus. The properties of these neurons suggest that they are involved in highly elaborate computations involved in representing the animal's position in space. Grid cells in particular have been hypothesized to perform a calculation using information about the animal's movement (proprioception, vestibular information, and optic flow) to form and update a unique code for relative position (McNaughton et al. 2006). Several classes of models have been proposed for how this "path integration" is accomplished.

One class of models extends an earlier model for keeping track of head direction with rotational movement information (Skaggs et al. 1995) to two-dimensional position (Samsonovich and McNaughton 1997). These models propose that a specific pattern of connectivity of a group of neurons results in a quasicontinuous "attractor," which stabilizes activity, and is thus able to keep a representation of a variable, such as position, in the absence of external input. To update this representation with rotation (in the case of the head-direction attractor), or translation (in the case of the position attractor), another group of neurons, which contain information about both head direction (or position) and rotation (or translation) interacts with the attractor network and moves the activity from one "attractor state" to another. This combined network "integrates" translational movement to calculate relative position. Grid-like activity results when periodic boundary conditions are applied to this model.

A second class of models makes use of the oscillatory properties of a major class of neurons in the MEC and suggests that if the information about the speed of movement is carried in the frequency of this oscillation, then the interference of this oscillation with another reference oscillation will give information about relative position (O'Keefe and Burgess 2005). One major difference in the practical implementation of this second class of models is that it does not allow the representation of a two-dimensional variable, such as position, without an intermediate step. The interference pattern of multiple (2 or more) oscillations can generate a grid pattern such as that exhibited by grid cells; however, the electrical properties of neurons do not allow them to carry multiple oscillations with different frequencies and phases (Remme et al. 2009). This means that each oscillation must be carried by a different neuron, and the summation carried out in stages.

One possible consequence of the interference of oscillations occurring in stages is that neurons that indeed represent one-dimensional position information exist. These neurons would fire in a "band-like" pattern when an animal traversed an environment, so that when the animal ran along one dimension of the environment, the neuron would alternate between rapid firing, and low or no firing, and in the orthogonal dimension the firing rate would remain the same (for a model using such cells see Mhatre et al. 2012). The summation of the inputs from three of these "band" cells, each with bands oriented at 60 degrees from one another, would result in the firing pattern already demonstrated by grid cells. Krupic et al. (2012) recently reported that the firing patterns of some medial entorhinal and parasubicular cells resemble those of these hypothesized "band cells."

Address for reprint requests and other correspondence: B. L. McNaughton, The Univ. of Lethbridge, 4401 Univ. Dr. W, Lethbridge, AB, T1K 3M4, Canada (e-mail: bruce.mcnaughton@uleth.ca).

Unlike the oscillatory interference model, continuous attractor networks can naturally represent either a one-dimensional variable or a two-dimensional variable such as position. To represent a one-dimensional variable such as head direction, the neural connectivity is arranged so that the neurons form a virtual line (or circle) with symmetrical connectivity along the line, and a two-dimensional variable is represented with the neural connectivity arranged so that the neurons form a virtual sheet with connectivity to all neighbors. This sheet is wrapped around both edges to form a torus to allow for the continuous repetition of firing fields shown by grid cells. Thus, the continuous attractor class of models favors representation of position immediately in two dimensions, with no intermediate one-dimensional stage, and did not predict band cells (but is not incompatible with the existence of band cells). The oscillatory interference model would be greatly supported by the existence of band cells, but alternate forms of the model may also be implemented without band cells (Welday et al. 2011).

Thus, Krupic and collegues' finding is a potentially significant development in the field, and proof of the existence of band cells would further the understanding of path integration mechanisms. We hypothesized, however, that the appearance of spatial band-like patterns could instead be achieved with the summation of grid firing patterns. Fyhn et al. (2007) showed that MEC grid cells recorded on the same tetrode show the same spacing and orientation of their grids, but different phases (position offsets) of the firing fields. We hypothesized that considering spikes from two grid cells recorded from the same tetrode, with the same spacing and orientation but different offset, as one unit would result in a spatial firing pattern that resembled "spatial bands." We simulated what would happen when clusters contaminated with spikes of a neighboring grid cell were analyzed in the same manner as in Krupic et al. (2012). Furthermore, we review methods for single cell isolation and determining the contamination level of "single" units, and make some recommendations for analyses that would provide better proof that the firing patterns observed by Krupic et al. constitute well-isolated band cells.

METHODS

Grid cell simulations. Activity of simulated grid cells was generated using position data from a rat randomly foraging in a 1 × 1-meter box during hippocampal recordings. The position of the rat was determined from a circular set of lights on the head stage connected to a hyperdrive implanted over the rat's head and recorded on an overhead camera. For each time frame of the video (60 frames/s), a circle was fit to the active pixels in the video, and the center of this circle was counted as the rat position. Noise in the video was removed by considering only pixels within a small radius of the position in the previous time frame.

For each simulated grid cell, an independent hexagonal grid pattern was defined in space, and the number of spikes generated by the cell was calculated based on the rat's location for each point in time. The probability a simulated cell would generate a spike depended on the distance from the nearest vertex at that point in time. Specifically, the probability of a spike at time t, p_t, was:

$$p_t = Ke^{-x/\tau}$$

where K was the maximum probability of generating a spike at a given location (K = 0.012–0.12/video frame, frame duration 16.7 ms), x was the distance to the nearest grid vertex, and τ was 20% of the distance between vertices. τ was set to 20% to approximate the field width observed in grid cells recorded in MEC.

Contaminated "units" were created by combining spikes from two simulated cells with varying spiking probabilities. For example, spikes from a simulated grid cell with K = 0.12 were combined with spikes from a simulated cell with K = 0.06 to create a 33% contaminated cell. Grid patterns of combined cells had the same orientation and periodicity but different spatial phase.

Spike trains generated as described above were then used for standard grid cell analyses. The position of the rat and the locations where each spike was fired were plotted (Fig. 1*A*); spatial firing rate maps were computed (Fig. 1*B*) and used to generate spatial autocorrelations (Fig. 1*C*), and gridness scores were calculated.

Gridness score. Grid scores were calculated as in Sargolini et al. (2006) and Langston et al. (2010). The autocorrelogram of the smoothed and occupancy normalized spatial firing plot was calculated, and a circular sample centered on the central peak (with the central peak removed) was used to calculate the grid score. This score is the maximum difference between the correlations of the circular sample at 60- and 120-degree rotations vs. 30-, 90-, and 150-degree rotations. The original "gridness" score designed by Sargolini et al. (2006) used a circular sample of the autocorrelogram defined by the first six peaks (outside of the central peak). Because cells that are less grid-like do not have six clear peaks at the same spacing in the autocorrelogram, Krupic et al. (2012) found the first peak and expanded the circle to 2.5 times that distance. Langston et al. (2010) used a different method to calculate grid scores for poorly defined grid cells of young rats, which was to calculate a grid score for each circular sample between 10 and 10 cm less than the width of the box, and use the maximum. Each method calculates different values of grid scores, but they are correlated (Langston et al. 2010). To calculate the significance of the grid score, the timing of the spikes is offset by random values (>20 s), and the resulting spike trains (and the semirandom positions of the animal at those spike times) are used to calculate a distribution of grid scores. Any grid score above the 95-percentile value of the grid scores from randomized spike trains is considered significant. Using the same method, we calculated a distribution of randomized grid scores with our simulated units for the Sargolini et al. (2006) peak-based grid score and the Langston et al. (2010) best radius-based grid scores and found 95-percentile thresholds of 0.13 and 0.43, respectively.

Fast-fourier transform. The periodicity of the spatial responses of clusters was estimated using a two-dimensional Fourier transform of the unsmoothed firing rate map (Krupic et al. 2012). The unsmoothed map was represented in a 64 × 64 array (corresponding to 1.5-cm^2 bins) with the mean value subtracted from each bin. The array was then zero-padded out to 256 × 256, to increase spatial resolution, and then the Fourier transform was applied. The two-dimensional Fourier spectogram was shifted such that low frequencies were at the center, and higher frequencies were in the periphery.

Grid cell recording. Extracellular recording was performed in a Long Evans rat using a chronically implanted 12-tetrode "hyperdrive" (see, e.g., Navratilova et al. 2012). All animal procedures were performed in accordance with the animal care guidelines issued by the government of Belgium and approved by the institutional welfare body at KU Leuven. The hyperdrive was implanted 3.6 mm laterally in the right hemisphere, 0.2–0.3 mm anterior to the transverse sinus, and at an angle of 10° to the sagittal plane in the anterior direction. Tetrodes were gradually lowered to 2.5–3 mm below the brain surface over 1–2 wk. The rat was trained to forage for chocolate and was kept at 85% of free-feeding body weight. Recording was performed in an open planar area, with area of movement limited only by the length of recording wires. A single boundary existed at the edge of the foraging area. Foraging radius was ~1.7 meters.

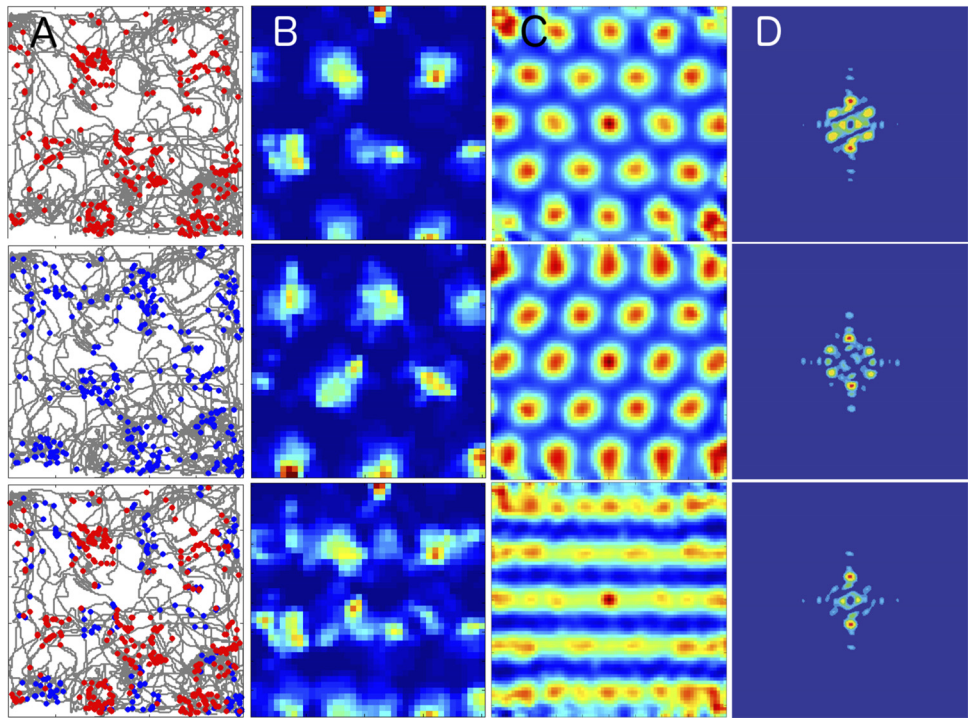

Fig. 1. Numerical simulation of spatially periodic bands arising from overlap of the grid fields of two poorly isolated or possibly physiologically coupled grid cells. *A*: position data from a rat foraging randomly in an environment is used to create a simulated spike distribution from two grid cells (red and blue). The spikes from *cell 1* (red) are combined with 50% of the spikes from *cell 2* (blue), to generate a "unit" containing 33% contamination. *B*: smoothed and occupancy normalized firing rate distributions of the spikes from the simulated cells and the combined contaminated unit. The firing rate color scale ranges from 0 (blue) to 5 (dark red) Hz in all images. *C*: spatial autocorrelogram of the smoothed firing rate distributions. *D*: 2-dimensional Fourier transform of the clean and contaminated units, calculated as in Krupic et al. (2012).

"Bandiness" analysis. To examine the band-like response of cells reported by Krupic et al. (2012), the smoothed position maps and corresponding Fourier plots (Krupic et al. 2012, Supplementary Fig. 10) were rotated until lines in the autocorrelogram were horizontal. With the use of image manipulation software (www.gimp.org), a rectangular section was taken from the rotated map at each location corresponding to a periodic band. A reverse mapping was made between the color of the position map and the map intensity. With the use of reverse mapping, the average intensity of each band was plotted as a function of position along the band.

RESULTS

To determine if units contaminated by one or more grid cells could create firing patterns that appear band-like, we simulated firing of grid cells with different relative offsets and combined them in different ratios. The firing patterns were simulated along a route followed by a rat during foraging for chocolate sprinkles randomly distributed in a 1-meter square box. An example firing pattern of two simulated cells is shown in Fig. 1*A*. The firing peaks of these two cells were offset from each other by 50% of the grid spacing along the horizontal axis (one of the three major axes of the rhomboidal grid) and by 8.8% along the vertical axis (which represents a 10-degree shift from the major axis). The spikes from each cell are combined in a ratio of 2:1, generating a unit that is 33% contaminated from spikes of a second cell. This level of contamination by such a cell generated a firing pattern that showed many peaks, oriented approximately along several parallel lines, resembling bands (Fig. 1*B*). The autocorrelation of the spatial firing pattern of this "unit" appeared very band-like (Fig. 1*C*).

We calculated the Fourier spectrograms for the simulated contaminated units as in Krupic et al. (2012). This calculation is essentially decomposing the spatial firing pattern into band patterns at different scales and orientations (Krupic et al. Fig. 1*F*). Grid cells should show six peaks in this plot, corresponding to the orientation of the three major axes of the hexagonal grid, and the spacing between grids. This indicates that a grid pattern could be conceptualized as the summation of three band patterns of the same scale, oriented at 60 degrees from one another but, of course, says nothing of how the pattern was generated in the brain. For a band-like spatial firing pattern, the Fourier spectrogram would show only two peaks. As shown in Fig. 1, however, the summation of two grid cells with the same spacing and orientation but an offset along (or almost along) one major axis will result in the Fourier components corresponding to that axis being stronger than the other two major axes (Fig. 1*D*).

"Grid scores" for simulated units were calculated as in Sargolini et al. (2006) and Langston et al. (2010). This grid score is the maximum difference between the correlations of a circular sample of the autocorrelogram of the spatial firing plot at 60- and 120-degree rotations, vs. 30-, 90-, and 150-degree rotations (see METHODS for details). Each method chooses a circular sample in different ways and calculates different values of grid scores, but the scores from different methods are correlated (Langston et al. 2010). Krupic et al. (2012) used a third method (see METHODS) to choose the circular sample. With each method, grid scores for randomized spike trains are also calculated, and any grid score above the 95-percentile score of the randomized spike trains is considered significant. We calculated a distribution of randomized grid scores for our simulated units using the Sargolini et al. (2006) peak-based grid score and the Langston et al. (2010) best radius-based grid score and found 95-percentile thresholds of 0.13 and 0.43, respectively. The grid score for the example contaminated "cell" in Fig. 1 is −0.04 when calculated according to the method in Sargolini et al. (2006) and 0.33 when calculated as in Langston et al. (2010), both of which are below the respective significance level, and thus this unit would be considered a

spatially periodic nongrid cell by Krupic et al. (2012). For the remainder of the simulations, grid scores calculated with the Sargolini et al. (2006) peak-based method are used, since these were more similar to the calculation Krupic et al. (2012) used, and the distribution of scores for randomized spike trains was more Gaussian with this measure.

Simulated unit contamination levels were varied between 10 and 50% to determine how much contamination is needed for the appearance of bands. An example of a unit increasingly contaminated by a cell with 50% offset is shown in Fig. 2. Bands appear in the autocorrelogram at a contamination of 25%, and the grid score becomes nonsignificant at a contamination of 33%. The Fourier spectrogram shows two main peaks at a contamination of 25%, and the other four peaks disappear by 40% contamination (data not shown). Units with the same contamination and offset parameters were simulated two times (with a different Poisson spike train) for each of two paths, and all four simulations at 40% contamination had nonsignificant grid scores. In one case, 25% contamination was enough for a nonsignificant grid score.

The relative offset of the primary grid cell and the contaminating grid cell is a major determinant of whether the resulting unit will appear grid-like, band-like, or some other pattern. We used contaminating grid cells with several offsets and observed that offsets of up to 15% resulted in units with firing patterns and grid scores indistinguishable from those of clean units, whereas offsets of 35% or more resulted in lower, sometimes nonsignificant, grid scores, an appearance of bandiness, and decreased hexagonal symmetry in the Fourier transform (Fig. 3). The three "prototypical" offsets are little or no offset (Fig. 3*A*, *bottom left*, and Fig. 3*Bi*), which would result in grid patterns and six peaks in the Fourier transform, 50% offset along a grid axis (and little or no offset in the orthogonal axis; Fig. 3*A*, *bottom right*, and Fig. 1), which would result in band-like patterns and two peaks in the Fourier transform, and 50% along a nongrid axis (30-degree shift from the grid axis; Fig. 3*A*, *top right*, and Fig. 3*Biv*), which would result in honeycomb-like patterns and six peaks in the Fourier transform, occurring at two spatial frequencies (if a large enough portion of the pattern is sampled). Examples of simulations with the most band-like patterns are shown in Figs. 1 (50% horizontal offset, 8.8% vertical offset) and 2 (45% horizontal offset, 0% vertical). The orientation and periodicity of the grid are the same for all grid cells recorded on the same tetrode (Fyhn et al. 2007; Stensola et al. 2012), and thus were not varied.

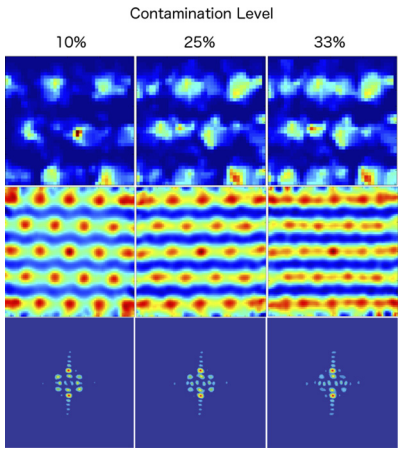

Fig. 2. Increasing contamination from a second grid cell increases the appearance of a band-like pattern. Contaminations of 10, 25, and 33% are shown. *Top*, smoothed firing rate plots contain several bumps, corresponding to firing fields of two cells. The firing rate color scale ranges from 0 (blue) to 5 (dark red) Hz in all images. *Middle*, autocorrelograms also contain multiple bumps. *Bottom*, as a result of the contamination, two or more peaks in the Fourier transform become weaker. Grid scores for these simulated units decrease from 0.39 and 0.27 (significant gridness) to 0.049 (below the 95 percentile of shuffled data).

Even though many of our simulated units appeared band-like in the autocorrelogram, and showed only two peaks in the Fourier transform, passing the criteria for "spatially periodic nongrid cell," it was still evident that the spatial firing pattern of these units did not form clean bands. There were multiple peaks in the spatial firing plot, indicating multiple fields, rather than bands. An analysis of the firing rate along each of the bands formed by combining simulated grid cells revealed repeating peaks of high firing rate (Fig. 4, *C* and *D*), unlike a simulation of a band cell (Fig. 4*E*). Thus, we performed a similar analysis of the Krupic et al. data to determine if their "band-like cells" resembled actual bands, with uniform firing rate along one axis, or a combination of many fields arranged in a band. The nine best examples of band-like cells, compiled in Krupic et al.'s Supplementary Fig. 10, all contained multiple peaks along each band (Fig. 5).

There are few reliable methods for estimating the contamination of a unit isolated from tetrode recordings (see DISCUSSION). The only method that does not rely on the same measures that are used for spike sorting is to check the number of spikes that occur within the refractory period of another spike. Hill and colleagues (2011) derived an equation for estimating the number of expected refractory period violations (r) of an isolated cluster with a given false positive (contamination) rate (c), which is as follows:

$$r = \frac{2(\tau_R - \tau_C)\, N^2 (1 - c) c}{T}$$

where τ_R is the length of the refractory period, τ_C is the censored period following a spike during which spikes are not detected by the recording system, N is the number of spike events clustered as part of the unit, and T is the total length of the recording during which spikes are detected. From this equation, we derived an estimate of the contamination of a unit:

$$c = \frac{1 - \sqrt{1 - \frac{4 \times p}{F \times 2.5\ \text{ms}}}}{2}$$

where F is the firing rate of the unit (N/T), r has been replaced with the proportion of refractory period violations ($p = r/N$), and $\tau_R - \tau_C$ has been replaced with the typical values used in recordings in our laboratory ($\tau_R = 2$ ms; $\tau_C = 0.75$ ms). This shows that the contamination rate of the unit depends not only on the proportion of refractory period violations, but also on the firing rate of the unit. Units with low firing rates are expected to show very few refractory period violations, even at high contamination rates. Labo-

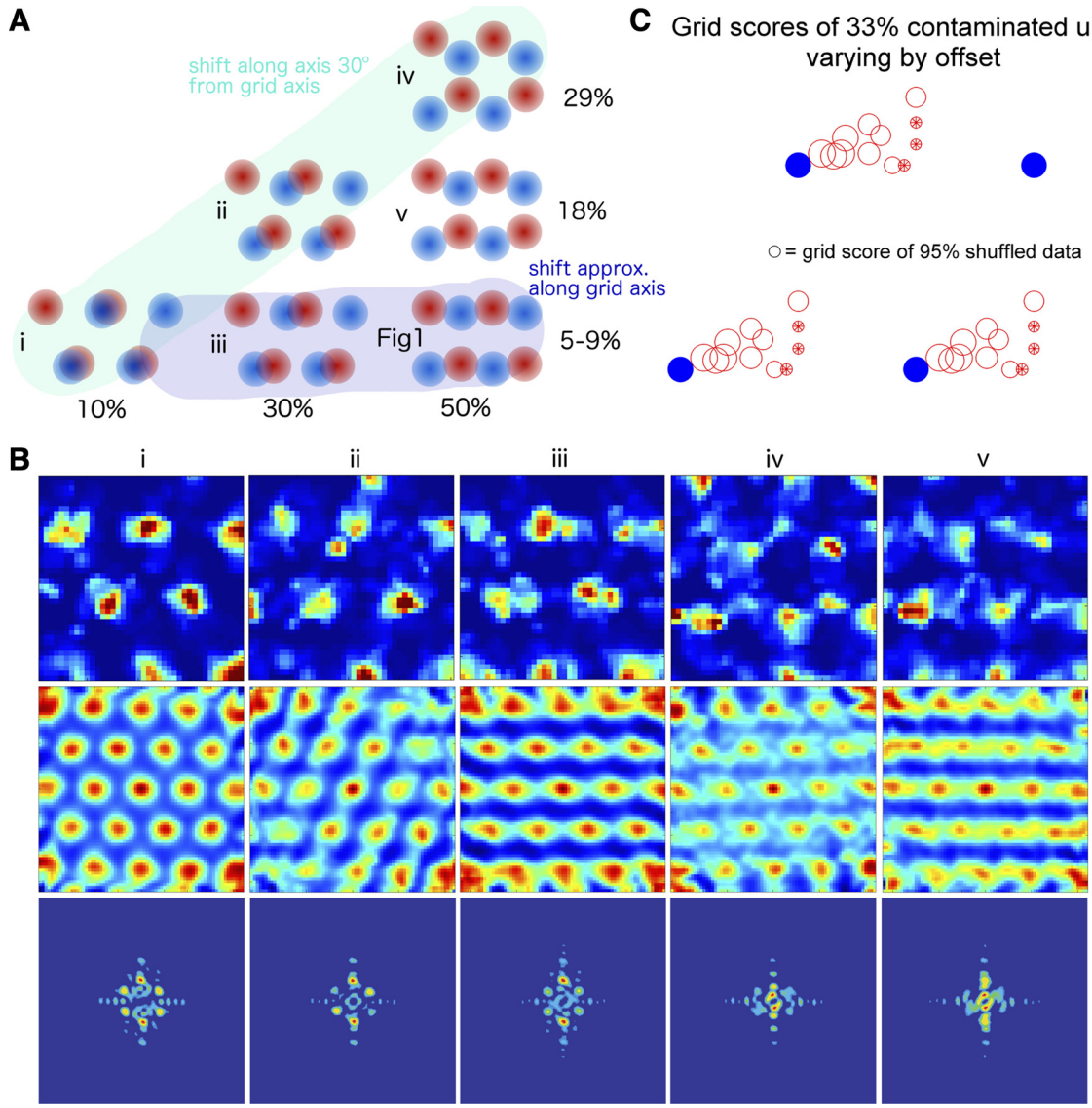

Fig. 3. Varying the offset and the direction of the offset of the contaminating grid cell results in varying "gridness" scores, a varying appearance of "bandedness," and different numbers of peaks in the spatial Fourier transform. *A*: schematic of mixtures of two grid cells with different offsets from each other. The component of the offset along the *x*-axis (one of the axes of the grid pattern) is expressed in percent of grid spacing, and the offset along the orthogonal axis is expressed as an angle from the *x*-axis. (The columns correspond to 10, 30, and 50% *x*-axis offsets and the rows to ~29, 18, and 5% *y*-axis offsets.) *B*: examples of spatial firing (*top*), spatial autocorrellograms (*middle*), and spatial Fourier transforms (*bottom*) of units with 33% contamination from cells with *offsets i–v* shown in the panel. The firing rate color scale ranges from 0 (blue) to 5 (dark red) Hz in all spatial firing rate images. *A*: the prototypical examples are i (almost perfect grid) and iv (perfect honeycomb). *Unit ii* is an example of a contamination of medium offset along a nongrid axis [30% *x* (grid)-axis offset, and 17.3% *y*-axis offset], which distorts the grid somewhat, but the gridness score is still significant. *Unit v* contains a contamination with large offset along a nongrid axis (50% *x*-axis offset, 18.2% *y*-axis offset), which results in a more zigzag, rather than band-like, pattern, but the grid is distorted enough to make the gridness score nonsignificant, and only one axis on the Fourier transform shows significant peaks. The Fourier transforms also show artifacts relating to the enclosure walls and the fact that only a small portion of the spatial pattern is sampled. *C*: gridness score as a function of offset for all simulated units containing 33% contamination (red circles). Simulated "clean" grid cells are also plotted (blue circles). The size of the circle indicates the average gridness score of all simulations at that offset and 33% contamination. Gridness scores that are not significantly different from random are also marked with an asterisk. Each simulation was repeated for two different paths through the environment and 1–4 times with different Poisson distributions of spikes. (Thus each point is the average of 2–8 simulations.) All average grid scores of contaminated and clean units are plotted repeatedly, to illustrate the pattern of the grid. This figure illustrates that contamination of a grid cell (with vertices at the blue circles) with spikes from another grid cell (with vertices at one set of red circles) results in nonsignificant gridness scores at certain grid field offsets but significant gridness at other offsets.

ratories vary widely in how they report cluster isolation quality and refractory period violations (see DISCUSSION), but often a threshold of maximum proportion of refractory period violations is used as a criterion, without considering the firing rate of the unit. As can be seen in Fig. 6*A*, even the conservative value of 0.2% of refractory period violations actually indicates an unacceptably high contamination rate when used for units with mean firing rates of <5 Hz. The accepted proportion of refractory period violations should actually be scaled with the firing rate of the cluster, depending on the desired maximum contamination rate according to the relation:

$$p = (c - c^2) \times F \times 2.5 \text{ ms}$$

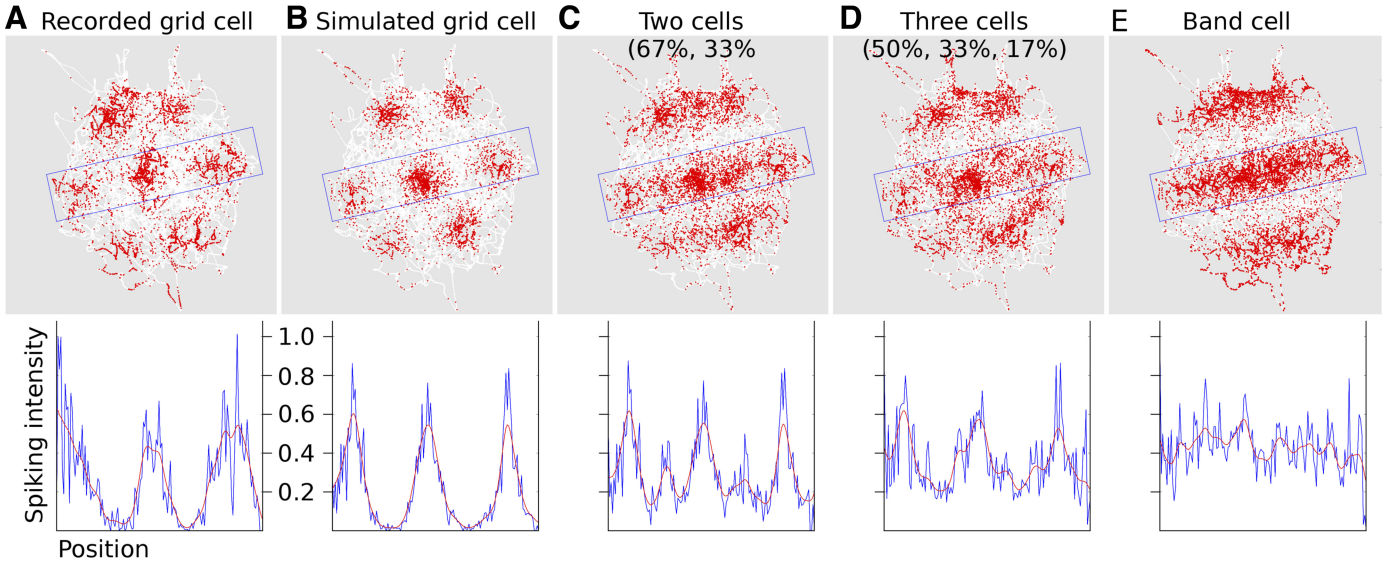

Fig. 4. Comparison of spiking distributions for a grid cell, simulated grid cells with various contaminations, and a hypothetical band cell. *A*: spiking activity of a recorded grid cell. White line indicates the position of the animal over time. Red shows the locations when this cell spiked. The overlaid rectangle outlines a slice that was analyzed for band-like behavior. *Bottom*, relative spiking response as a function of location along the long axis of the rectangle (no. of spikes divided by occupancy). Red line is the firing rate smoothed with a 4- to 6-cm kernel. *B*: a simulated grid cell. Simulated spikes were generated based on position, using the same tracking data as recorded in *A*. Analysis rectangle is the same as in *A*. *C*: the summed spikes of two simulated grid cells. Spikes were generated for two grids, both aligned with the long axis of the analysis rectangle, with vertices 50% offset; 67% of spikes come from one grid cell, and 33% are from the other. *D*: the summed spikes of three simulated grid cells. Three grids with vertices aligned along the analysis rectangle and offset 33 and 67% from one another were simulated; 50% of spikes come from one grid cell and 33 and 17% from the other two. *E*: a simulated band cell. Spikes were generated in the same way as in *B–D* except, instead of distance from the vertex of hexagonal grids, the distance from 3 lines aligned with the analysis rectangle was used. The result shows a band of spiking activity (*top*) with no periodicity and smaller variance to mean ratio (*bottom*) than the cases in which apparent bands are the result of grid superposition.

which is plotted in Fig. 6*B*.

Another criterion used to evaluate refractory period violations is the $R_{2:10}$ value proposed by Fee et al. (1996). This calculation involves comparing the rate of refractory period violations with the rate of spikes within $\tau_C - 10$ ms of another spike according to the equation:

$$R_{2:10} = \frac{(10\text{ ms} - \tau_C)}{(\tau_R - \tau_C)} \times \frac{p}{F_{10}}$$

If we assume that $F_{10}/(10\text{ ms} - \tau_C)$ is similar to the firing rate of the unit, we can also use $R_{2:10}$ to estimate the contamination rate as:

$$c \approx \frac{1 - \sqrt{1 - 4 \times R_{2:10}}}{2}$$

This suggests that, for a maximum contamination of 10%, only units with $R_{2:10} \leq 0.09$ should be used. Of course, the rate of spikes within 10 ms of another spike is higher than the baseline firing rate of a bursting neuron, and thus $R_{2:10}$ provides an (often large) overestimate of the contamination rate of bursting cells.

Krupic et al. (2012) do not report the criterion of refractory period violations they used, and thus we cannot comment on the contamination levels of their units. Another important caveat is that the refractory period criterion is based on uncorrelated Poisson spike trains. However, two grid cells with perfectly offset fields are expected to have a negative correlation. In this case, even the refractory period violation criterion does not aid in determining the isolation quality. This is a general issue for units that may have intrinsic nonzero correlations.

DISCUSSION

Spike sorting methods. While tetrodes provide superior isolation of single units compared with most single channel electrodes, and hence facilitate extracting activity of many single neurons simultaneously, the isolation of single neurons is still difficult and for most units cannot be accomplished perfectly. This method involves detecting action potentials from extracellularly recorded electrical potentials. Bandpass filtering is used to detect signals in the frequency band of action potentials, and, most commonly, an amplitude filter is used to detect these spikes. To identify the spikes from single neurons, the waveform shapes and amplitudes on the four channels of the tetrode are used to classify different neurons (Gray et al. 1995). Different spike sorting algorithms use slightly different measures of the waveforms, but, generally, each waveform is decomposed into two to four features that are most representative of the spike. Usually this is done with principal component analysis (PCA) of the full waveforms of all recorded spikes on an electrode, and the first and second principal components (PCs) are used for sorting. The first component usually corresponds to the amplitude of the waveform (Harris et al. 2000; e.g., Lewicki 1998), which can also be replaced with a measure of the peak amplitude, the peak-to-trough height, or the energy of the waveform (the root mean square of all samples taken along the waveform). The second component corresponds to features of the second half of the spike waveform (Harris et al. 2000; e.g., Lewicki 1998), since the spikes vary in width and amount of afterhyperpolarization. In algorithms where energy is used instead of the first PC, the waveforms are energy normalized before PCA, and thus the first PC corresponds to the waveform shape, similar to the

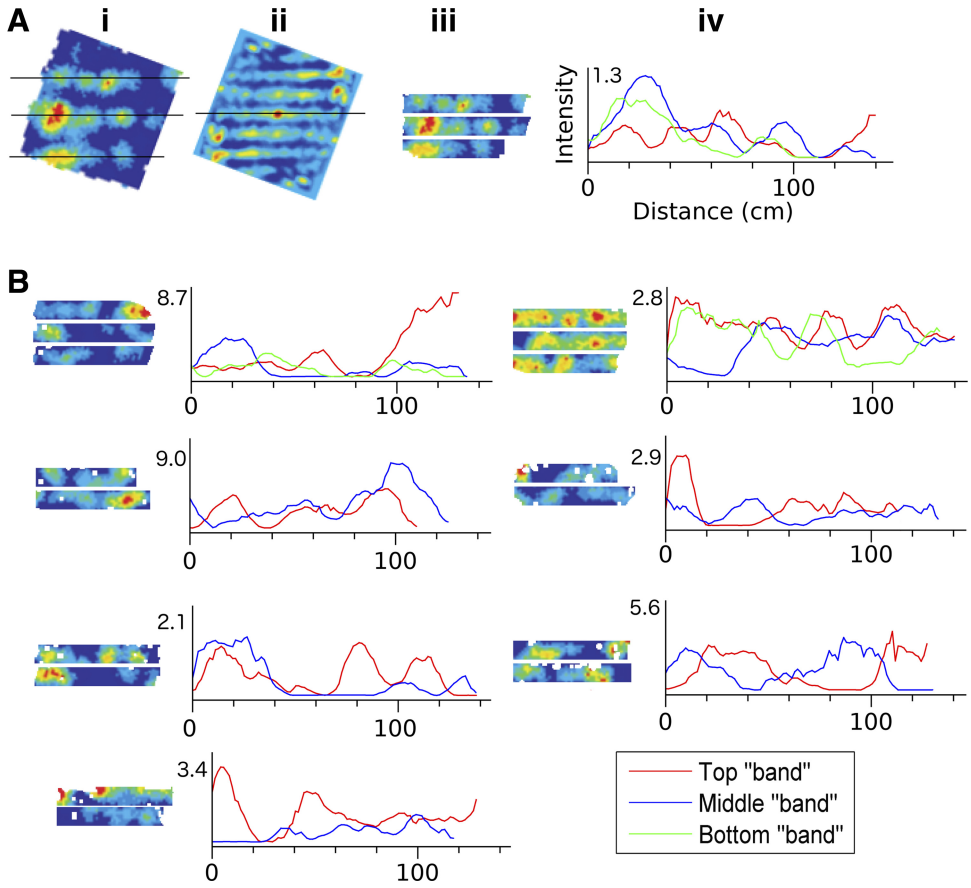

Fig. 5. Periodic firing rate modulation within bands recorded by Krupic et al. suggests the summation of multiple fields. *A*: an analysis of firing rate along the bands was conducted on the best 8 examples from Krupic et al. (2012). Cells with band-like behavior were taken directly from their Supplementary Fig. 10 and rotated so the axis of the "band" in the firing rate plot (i) and spatial correllogram (ii) was horizontal. Each band was extracted from the firing rate maps (iii), and the firing rate (intensity) along this band was estimated by converting the color map (iv). *B*: if these activity patterns represented bands from hypothesized band cells, the intensity of activity should be largely uniform across the length of the band. Instead, the activity within each purported band is variable, and usually periodic. The maximum firing rate (in Hz) from each firing rate plot in Krupic's Supplementary Fig. 10 is displayed on the *y*-axis of our converted intensity plot.

second PC described earlier (e.g., Schmitzer-Torbert et al. 2005). Finally, these features of the waveforms are used (either manually, or with an automated algorithm) to sort spikes into clusters that roughly correspond to single neurons (called units, because single cell isolation cannot be completely confirmed). Automated algorithms often operate under the assumptions that clusters are Gaussian in shape (but see Fee et al. 1996, Quiroga et al. 2004, Takekawa et al. 2010), spikes and the underlying "noise" are independent, and background noise is stationary. These assumptions are sometimes violated (in particular the Gaussian clusters assumption, see below), and thus a manual step in which a user corrects the clusters generated is often included. Manual correction of automated clustering is easiest if the automated algorithm overclusters the data, and the experimenter then merges clusters that have similar spike shapes and cross-correllograms indicative of a single neuron.

Two types of problems are encountered when sorting spikes: incorrectly excluding spikes fired by the recorded neuron (false negatives, type II error) and incorrectly including spikes not fired by the neuron in the cluster (false positives, type I error). The reasons for false negatives are: exclusion of spikes when background noise in the recording causes the spike amplitude to drop below the detection threshold, exclusion of spikes

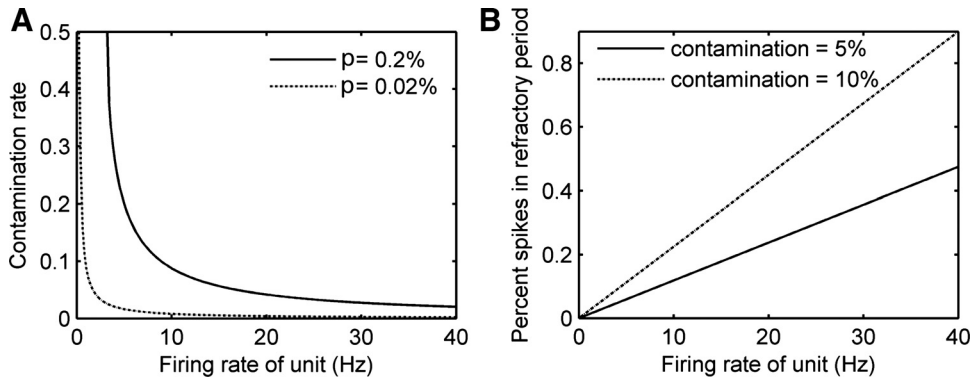

Fig. 6. Assuming Poisson firing statistics and uncorrelated tuning curves of neurons, the false positive rate (contamination rate) of a unit can be estimated from the number of spikes occurring during the refractory period following another spike (see text). *A*: false positive rate as a function of firing rate of the cluster given an accepted percentage of 0.2 and 0.02% spikes in the refractory period (p). Note that a contamination rate of 0.5 (50%) indicates a cluster containing 50% true spikes and 50% spikes from other neurons. *B*: the acceptable percentage of spikes in the refractory period should vary based on firing rate of the unit and the experimenter's accepted false positive rate, for example, 5 or 10%, as plotted here.

when multiple recorded neurons fire in close temporal proximity, resulting in a compound spike waveform that is undetectable or unclassifiable (Harris et al. 2000; Lewicki 1998), and incorrect classification of spikes from one cell to the cluster of another cell because of similarity in waveforms. The analysis of a unit with many false negatives will result in incorrect calculation of firing rate, and receptive fields will appear to have smaller amplitudes (Hill et al. 2011). Reasons for including false positives in a cluster are: the incorrect segregation of two or more cells with similar waveform shapes and amplitudes and misclassification of composite spikes or noise in the recording as spikes from a single neuron. The analysis of a unit with many false positives also results in an incorrect calculation of firing rates and, additionally, in an incorrect characterization of the receptive field (Hill et al. 2011), such as what is modeled in this paper.

The likelihood of spike sorting errors increases when there are large numbers of spike overlaps. Spike overlaps increase during population burst events such as sharp waves (SPWs), or when two of the cells recorded on a tetrode are coupled, and therefore often spike in rapid succession. Additional problems occur when the assumptions of the spike sorting algorithms are violated. For example, spike waveform shapes and amplitudes are known to change within a burst, violating the assumption that waveforms only vary with Gaussian noise (e.g., Harris et al. 2000). In addition, if the position of a tetrode drifts during a recording, the recorded spikes will change as well. These problems require users to manually adjust the results from automated clustering algorithms but often cannot be assessed quantitatively.

Resulting spike clusters may include both false positive and false negative errors, and the larger the proportion of each, the noisier any subsequent analysis will be. It is therefore important to determine the quality of unit isolation, to be able to evaluate the significance of any analysis that assumes single cell isolation. In an experiment in which spike sorting from tetrode recordings was evaluated with knowledge of the true spike times of a cell that was also recorded intracellularly, manually cut clusters contained somewhere between 0 and 30% errors, depending on the recorded amplitude of the spike (which corresponds to the inverse square of the distance between the tetrode and the neuron) and the experience of the cluster cutter (Harris et al. 2000). Better results were achieved with a semiautomated algorithm (in which the automated algorithm delineates clusters in multidimensional space, and then the human operator merges overclustered units) up to a theoretical limit determined again by the strength of the signal and the degree of violation of the assumptions of the algorithm the cell displays, including burstiness and overlapping spikes. Without simultaneous intracellular recordings, the true cell classification of spikes cannot be known, and thus any measures of isolation quality or errors are only estimates. The strength of the signal can by quantified by the signal-to-noise ratio (S/N), which determines how good the recording of a particular neuron will be and can be used to ensure that spikes will not be excluded because they do not pass the threshold of detection due to noise in the recording (Lemon 1984). This metric does not, however, quantify the proportion of undetected spikes, nor does it measure whether spikes from two cells have been classified as one unit (Joshua et al. 2007).

Unit isolation measures. One way to evaluate cluster isolation quality is to use the same measures used to separate clusters (e.g., waveform shape and amplitude). Harris et al. (2001) suggested a metric called isolation distance to calculate the distance between a cluster and all the other spikes recorded on the same tetrode (in the 8-dimensional space defined by the energy and first PC of waveform shape on the 4 recording channels). This metric measures the distance from the center of an identified cluster that will contain all the spikes in the cluster and the same number of noise (noncluster) spikes. When used on the Harris et al. (2000) tetrode recordings, which also included intracellular recordings indicating the true result, the isolation distance of a cluster was found to correlate well with the false positives included in that cluster and very slightly, but significantly, with the number of false negatives (Schmitzer-Torbert et al. 2005). While this measure allows the comparison of the isolation of units recorded on a single tetrode, it is very dependent on the distribution of the noncluster spikes, and thus cannot be used to quantitatively compare values between tetrodes. For example, a cluster that is very close to one other smaller cluster, but far away from the rest of the spikes recorded on that tetrode, may earn a higher isolation score than a lower-amplitude cluster (closer to the multiunit noise) that is nonetheless farther removed from all other points. Therefore, it is not possible to design a criterion value of isolation distance that can be compared between experiments. Schmitzer-Torbert and Redish (2004) designed a different measure of cluster isolation, L-Ratio, which discounts noise spikes that are distant from the center of the cluster, providing a more accurate account of the distribution of noise spikes surrounding a cluster. This measure was found to correlate pretty well both with true false positives and true false negatives (Schmitzer-Torbert et al. 2005). Joshua et al. (2007) went a step further when defining their "isolation score" and quantified the local distances between points within the cluster and those outside. They also tested their score with a simulation of false positive and negative errors, which they used to suggest a threshold isolation score that would determine units suitable for further study. In addition to the isolation score, the authors designed separate calculations for estimating false positives and false negatives and determined that these estimates are likely to be accurate for units above the threshold isolation score. Their measures worked well in simulation but have not been evaluated with data for which the true false positive and false negative rates are known (Harris et al. 2000) and thus cannot be adequately compared with the two above-mentioned measures. One fault in common between all above measures is that they only use features also used in automated spike sorting and thus are subject to the same assumptions. For example, a cluster of a bursty cell may show a worse isolation score than two clusters made up of the high-amplitude (early in the burst) and low-amplitude (late in the burst) spikes from the same cell.

A method to detect false positive errors in spike sorting that is completely independent of the sorting method involves counting the spikes that occur during the refractory period following another spike in the same cluster. The spikes that occur during the refractory period cannot belong to the same cell, and thus the proportion of spikes showing a low (2–3 ms) interspike interval can be used to estimate the contamination of a cluster, under the appropriate conditions. This value has been

used in two main ways: calculating just the proportion of spikes that occur in the refractory period (Takehara-Nishiuchi and McNaughton 2008) or the ratio of spikes in the refractory period (2 ms within another spike) to spikes within 10 ms of another spike ($R_{2:10}$; Fee et al. 1996). Unlike the proportion of spikes in the refractory period, $R_{2:10}$ is an indicator of contamination that is independent of the firing rate of the unit (see RESULTS and below); however, bursting neurons increase their firing rate in the 10 ms following a previous spike, and thus this value is higher than the overall firing rate for those neurons. Harris et al. (2000) recommended comparing firing in the refractory period with the asymptotic value of the autocorrelogram (which is the firing rate) but did not suggest a quantitative criterion.

Krupic et al. (2012) do not report what criterion for refractory period violations was used in their study, but hippocampal electrophysiology studies in our lab typically exclude any units with a percentage of spikes in the refractory period greater than between 1 and 0.2%. The false positive rate can be calculated from the percentage of spikes occurring in the refractory period based on the expected probability that a rogue spike occurs around the spikes of the clean unit (Hill et al. 2011). From Hill and colleagues' equation, the false positive rate depends on the proportion of spikes occurring in the refractory period and the firing rate of the cluster (see RESULTS and Fig. 6). For a cell that fires at 10 Hz, 0.2% spikes in the refractory period represents a 5% false positive rate, but for a cell that only fires at 1 Hz (which is the average rate reported in the Krupic at al. study), 0.2% spikes in the refractory period would mean a false positive rate of >50% (see Fig. 6). From our experience, most low firing rate clusters would not show this high of a rate of refractory period violations, but this calculation illustrates that the criterion needs to be adjusted for cells with low firing rates. Furthermore, this calculation makes the assumption that contaminating spikes occur independently of spikes from the unit of interest, which is definitely violated when the contamination comes from another place-related cell. Two grid cells with non- or only partially overlapping fields (such as those we show in Figs. 1 and 2, which would sum to a band-like response) should show very little spike timing overlap, and thus in that case this calculation is a severe underestimate of the contamination rate. On the other hand, during SPWs spike timing overlap is higher than expected by chance, and so when epochs containing many SPWs are used for spike sorting, this calculation may be an overestimate of the false positive rate.

Additional methods of estimating false positives and false negatives include estimating the spikes missed as a result of the detection methods and measuring the overlap between each pair of clusters (Hill et al. 2011). The proportion of spikes that have not been detected based on a threshold spike amplitude (or any other detection method) can be calculated by plotting the distribution of the cluster around the detection threshold, fitting a Gaussian to the distribution, and calculating the proportion of spikes that would fall under the threshold but have not been detected (Hill et al. 2011). This problem should be reduced, however, by using only cells with a high enough S/N and setting an appropriate detection threshold. The other causes of undetected spikes are spikes that occurred during the detection of another spike (either because of spike overlap or because of the censored period following detection of a spike). The expected proportion of spikes missed in this way can be easily calculated (under the assumptions of Poisson spiking that is uncorrelated between neurons) from the firing rate of the cell, the total number of detected events, and the length of each censored period (Hill et al. 2011). Hill and colleagues (2011) suggest estimating the total number of false positives and false negatives by combining these measurements of undetected spikes, the measurement of false positives from refractory period violations, and a measurement of the probability of misclassifying each spike into another identified cluster. As complete as this calculation attempts to be, it is still only an estimate, since the statistics of spike timing are not strictly Poisson (and all the calculations dependent on expected rates of spikes assume Poisson statistics). Nonetheless, Hill et al.'s calculation captures the idea that no one measure gives a complete picture of the isolation quality of a unit and that strict criteria should be set and reported for inclusion of "well-isolated single units" in an analysis.

In conclusion, while methods to determine cluster isolation quality are still imperfect, the reporting of the use of such metrics is even more so. A literature search of the spike sorting metrics used in prominent laboratories in the in vivo electrophysiology hippocampal field indicated that very few papers actually report which specific criteria were used for evaluation of spike sorting quality. Many papers report qualitative criteria (e.g., "only units with clear refractory periods are included"), or which measure was used (e.g., isolation distance was calculated), without stating the criterion value(s), and many do not report which measures were used at all. As more laboratories use these techniques and more spike sorting methods are introduced, this standard will have to change, so that readers and reviewers can better evaluate the results and conclusions of a paper. Promising new spike sorting methods are being developed (e.g., Takekawa et al. 2010), which have yet to be tested with novel in vivo data, and there is a push for more automated methods (for review, see Rey et al. 2015). This makes it even more important to discuss isolation quality and come to some consensus on criteria.

Neuronal population analyses do not necessarily require perfect cell isolation (e.g., Davidson et al. 2009), but when making a statement about the receptive fields of single cells, extreme caution should be used to determine that the property in question is true of even the best isolated single units. We have shown in this paper that, given the current knowledge of grid cells, contamination of grid cell clusters would result in multipeaked spatial receptive fields that could be considered band-like. Because of the difficulty in ascertaining single cell isolation, and the simulation that we show here, we believe that Krupic et al. (2012) did not provide definitive proof of band-like cells in either of the two regions they recorded from (MEC and parasubiculum). To demonstrate that such cells exist, they would have to show several more rigorous analyses to prove that the units they claim are band cells are very well isolated, as well as that their Fourier transform analysis is reliable at identifying band cells. Krupic et al. (2012) claim that showing the mean isolation distance and L-Ratio measures for their "grid" and band-like cells proves that the two classes are equally well isolated. We show in Fig. 3, however, that contaminated clusters could also be classified as grid cells. We posit that poorly isolated units also contributed to the mean

isolation score for the "grid cell" class and suggest that the mean values of those measures are not definitive proof that the classes are equal, since it does not show the distribution of isolation metrics for each recorded unit. Showing this distribution or the correlation between isolation and gridness score would better illustrate whether any of the best-isolated units contribute to the finding of band-like cells. Krupic et al.'s observation that grid cells have greater between-session stability than spatially periodic nongrid cells (their Fig. 2) is consistent with our hypothesis that their band-like clusters are less likely to be well-isolated.

Finally, we show that Krupic and colleagues' raw data (spatial firing rate plots) show multiple peaks along the axis of each of their identified "bands" (Fig. 5), putting into question the reliability of their Fourier transform analysis for identifying bands. This analysis attempts to fit differently oriented and spaced band patterns to the spatial firing plot of units (see Krupic et al.'s Fig. 1*F*), and then interprets the presence of less than three peaks (which indicate grid cells) in the resulting Fourier plot as evidence of band-like firing. We found that the presence of spikes from other grid cells reduces the number of peaks in this spatial Fourier transform (Fig. 2) and that this measure becomes unreliable with increasing spacing of fields when only a few fields are observed in the environment (data not shown). Krupic et al. used data from units with few and very noisy fields in their analysis of the proportion of grid and band-like cells, without accounting for how unreliable the measurements on these units are. Their observation that spatially periodic nongrid cells show less precise Fourier component orientation tuning than grid cells (their Fig. 3) is consistent with our suggestion that many of their band-like cells are poorly isolated and/or sparsely spiking, resulting in a less reliable Fourier analysis. When they initially discovered grid cells, Fyhn et al. (2004) compared the waveforms of spikes in each of the regularly repeating fields to ensure that each field was in fact a result of firing of the identical cell and that their finding was not due to poor isolation (their Supplementary Fig. 3). Krupic et al. (2012) could show a similar analysis for the multiple peaks observed in the spatial firing plots of their band-like cells to convince us that our simulation results do not apply to their data. Therefore, we call on Krupic and colleagues to show better evidence of cluster isolation quality and analyze their best-isolated units for bandiness with a measure that includes a reliability estimate.

ACKNOWLEDGMENTS

We thank E. Moser for sharing Matlab code used in his laboratory for calculation of gridness scores.

Present address of K. B. Godfrey: Allen Institute for Brain Science, 615 Westlake Ave. N., Seattle, WA 98109.

GRANTS

This work was supported by a Polaris Award from Alberta Innovates Health Solutions, by a Discovery grant from the National Sciences and Engineering Research Council of Canada, and by an operating Grant from Neuroelectronics Research Flanders.

DISCLOSURES

No conflicts of interest, financial or otherwise, are declared by the authors.

AUTHOR CONTRIBUTIONS

Z.N. and B.L.M. conception and design of research; Z.N. and K.B.G. analyzed data; Z.N., K.B.G., and B.L.M. interpreted results of experiments; Z.N. and K.B.G. prepared figures; Z.N. drafted manuscript; Z.N., K.B.G., and B.L.M. edited and revised manuscript; Z.N., K.B.G., and B.L.M. approved final version of manuscript; K.B.G. performed experiments.

REFERENCES

Davidson TJ, Kloosterman F, Wilson AM. Hippocampal replay of extended experience. *Neuron* 63: 497–507, 2009.

Fee MS, Mitra PP, Kleinfeld D. Automatic sorting of multiple unit neuronal signals in the presence of anisotropic and non-Gaussian variability. *J Neurosci Methods* 69: 175–188, 1996.

Fyhn M, Molden S, Witter MP, Moser EI, Moser MB. Spatial representation in the entorhinal cortex. *Science* 305: 1258–1264, 2004.

Fyhn M, Hafting T, Treves A, Moser MB, Moser EI. Hippocampal remapping and grid realignment in entorhinal cortex. *Nature* 446: 190–194, 2007.

Gray CM, Maldonado PE, Wilson M, McNaughton B. Tetrodes markedly improve the reliability and yield of multiple single-unit isolation from multi-unit recordings in cat striate cortex. *J Neurosci Methods* 63: 43–54, 1995.

Hafting T, Fyhn M, Molden S, Moser MB, Moser EI. Microstructure of a spatial map in the entorhinal cortex. *Nature* 436: 801–806, 2005.

Harris K, Hirase H, Leinekugel X. Temporal interaction between single spikes and complex spike bursts in hippocampal pyramidal cells. *Neuron* 32: 141–149, 2001.

Harris KD, Henze DA, Csicsvari J, Hirase H, Buzsáki G. Accuracy of tetrode spike separation as determined by simultaneous intracellular and extracellular measurements. *J Neurophysiol* 84: 401–414, 2000.

Hill DN, Mehta SB, Kleinfeld D. Quality metrics to accompany spike sorting of extracellular signals. *J Neurosci* 31: 8699–8705, 2011.

Joshua M, Elias S, Levine O, Bergman H. Quantifying the isolation quality of extracellularly recorded action potentials. *J Neurosci* 163: 267–282, 2007.

Krupic J, Burgess N, O'Keefe J. Neural representations of location composed of spatially periodic bands. *Science* 337: 853–857, 2012.

Langston R, Ainge J, Couey J. Development of the spatial representation system in the rat. *Science* 328: 1576–1580, 2010.

Lemon R. Methods for neuronal recording in conscious animals. *IBRO Handb Ser Methods Neurosci* 4: 1–162, 1984.

Lewicki M. A review of methods for spike sorting: the detection and classification of neural action potentials. *Netw Comput Neural Syst* 9: R53–R78, 1998.

McNaughton BL, Battaglia FP, Jensen O, Moser EI, Moser, MB. Path integration and the neural basis of the "cognitive map." *Nat Rev Neurosci* 7: 663–678, 2006.

Mhatre H, Gorchetchnikov A, Grossberg S. Grid cell hexagonal patterns formed by fast self-organized learning within entorhinal cortex. *Hippocampus* 22: 320–334, 2012.

Navratilova Z, Hoang LT, Schwindel CD, Tatsuno M, McNaughton BL. Experience-dependent firing rate remapping generates directional selectivity in hippocampal place cells. *Front Neural Circuits* 6: 6, 2012.

O'Keefe J, Burgess N. Dual phase and rate coding in hippocampal place cells: theoretical significance and relationship to entorhinal grid cells. *Hippocampus* 15: 853–866, 2005.

O'Keefe J, Dostrovsky J. The hippocampus as a spatial map. Preliminary evidence from unit activity in the freely-moving rat. *Brain Res* 34: 171–175, 1971.

Quiroga RQ, Nadasdy Z, Ben-Shaul Y. Unsupervised spike detection and sorting with wavelets and superparamagnetic clustering. *Neural Comput* 16: 1661–1687, 2004.

Ranck JB Jr. Head direction cells in the deep layers of dorsal presubiculum in freely moving rats. 10: 599, 1984.

Remme MW, Lengyel M, Gutkin BS. The role of ongoing dendritic oscillations in single-neuron dynamics. *PLoS Comput Biol* 5: e1000493, 2009.

Rey HG, Pedreira C, Quian Quiroga R. Past, present and future of spike sorting techniques. *Brain Res Bull* 119: 106–117, 2015.

Samsonovich A, McNaughton BL. Path integration and cognitive mapping in a continuous attractor neural network model. *J Neurosci* 17: 5900–5920, 1997.

Sargolini F, Fyhn M, Hafting T, McNaughton BL, Witter MP, Moser MB, Moser EI. Conjunctive representation of position, direction, and velocity in entorhinal cortex. *Science* 312: 758–762, 2006.

Savelli F, Yoganarasimha D, Knierim JJ. Influence of boundary removal on the spatial representations of the medial entorhinal cortex. *Hippocampus* 18: 1270–1282, 2008.

Schmitzer-Torbert N, Redish AD. Neuronal activity in the rodent dorsal striatum in sequential navigation: separation of spatial and reward responses on the multiple T task. *J Neurophysiol* 91: 2259–2272, 2004.

Schmitzer-Torbert N, Jackson J, Henze D, Harris K, Redish AD. Quantitative measures of cluster quality for use in extracellular recordings. *Neuroscience* 131: 1–11, 2005.

Skaggs WE, Knierim JJ, Kudrimoti HS, McNaughton BL. A model of the neural basis of the rat's sense of direction. *Adv Neural Inf Process Syst* 7: 173–180, 1995.

Solstad T, Boccara C, Kropff E, Moser M, Moser E. Representation of geometric borders in the entorhinal cortex. *Science* 1109: 1865–1868, 2008.

Stensola H, Stensola T, Solstad T, Frøland K, Moser MB, Moser EI. The entorhinal grid map is discretized. *Nature* 492: 72–78, 2012.

Takehara-Nishiuchi K, McNaughton BL. Spontaneous changes of neocortical code for associative memory during consolidation. *Science* 322: 960–963, 2008.

Takekawa T, Isomura Y, Fukai T. Accurate spike sorting for multi-unit recordings. *Eur J Neurosci* 31: 263–272, 2010.

Taube JS, Muller RU, Ranck JB Jr. Head-direction cells recorded from the postsubiculum in freely moving rats. I. Description and quantitative analysis. *J Neurosci* 10: 420–435, 1990.

Welday AC, Shlifer IG, Bloom ML, Zhang K, Blair HT. Cosine directional tuning of theta cell burst frequencies: evidence for spatial coding by oscillatory interference. *J Neurosci* 31: 16157–16176, 2011.